Gd^{3+} EPR spectroscopy and optical microscopy study of ferroic states in $Cd_2Nb_2O_7$ pyrochlore

1998 J. Phys.: Condens. Matter 10 9309

(http://iopscience.iop.org/0953-8984/10/41/013)

J. Phys.: Condens. Matter **10** (1998) 9309–9316. Printed in the UK PII: S0953-8984(98)92439-0

Gd^{3+} EPR spectroscopy and optical microscopy study of ferroic states in $Cd_2Nb_2O_7$ pyrochlore

N N Kolpakova†, S Waplak‡ and W Bednarski‡

† A F Ioffe Physico-Technical Institute RAS, Polytekhnicheskaya Street 26, 194021 St Petersburg, Russia

‡ Institute of Molecular Physics PAS, Smoluchowskiego 17/19, 60-179 Poznan, Poland

Received 12 March 1998, in final form 14 July 1998

Abstract. The EPR spectroscopy (using Gd^{3+} as the EPR probe) and optical microscopy studies of $Cd_2Nb_2O_7$ pyrochlore were carried out in the temperature range of 80 K–300 K which included phase transitions at $T_s = 205$ K, $T_C = 196$ K and $T_{inc} = 86$ K. The evidence for coexistence of a *proper* ferroelectric–ferroelastic state and an *improper* ferroelectric–ferroelastic state in the ferroelectric phase of $Cd_2Nb_2O_7$ is presented. While the former appears below T_C, the latter comes from the improper ferroelastic state of the precedent phase ($T_C < T < T_s$). The unusual behaviour of the ferroic states on a temperature scale is discussed from the viewpoint of a two-weakly-bonded-network description of the pyrochlore structure.

1. Introduction

The fact that in $Cd_2Nb_2O_7$ pyrochlore ($Fd3m$-O_h^7) the domains with boundaries along the $[100]_{cub}$-type directions and the domains with boundaries along the $[110]_{cub}$-type directions coexist within about 10 K below the Curie temperature ($T_C = 196$ K) is not entirely new [1–4]. However, the nature of this phenomenon is unknown. While the $[100]_{cub}$-type domains appear below $T_s = 205$ K (a ferroelastic phase), the $[110]_{cub}$-type domains appear below T_C. The phase below T_C is characterized as a partial ferroelastic–partial ferroelastic ($\boldsymbol{P}_s \| [100]_{cub}$) [4]. Neither the nature of domains of this ferroic phase nor correlation between domains of this phase and ferroelastic domains of the precedent ferroic phase nor the mechanisms of the domain evolution on a temperature scale have been studied. To elucidate these questions, a study of true thermally induced changes in the domain pattern and characterization of both ferroic states from the structure-instability viewpoint need to be performed. On the other hand, elucidation of the nature of the ferroic states and of their evolution on a temperature scale is also of great importance for understanding the mechanism responsible for coexistence of the ordered (ferroelectric) and disordered (relaxor, incommensurable, glassy) states in $Cd_2Nb_2O_7$ [5, 6].

In nominally 'pure' $Cd_2Nb_2O_7$, the phase transitions (PTs) to the ferroic states are second order [4, 5, 7]. Under uniaxial stress or external dc electric field, the PT at T_s is a first-order PT close to the second-order one [3, 4]. From calorimetric studies, the PTs at T_s and T_C are of a mixed order–disorder and displacive character [5]. The displacive character of the PT at T_C is also confirmed by the fact of the existence of the IR-active soft mode above T_C and of the Raman-active soft mode below T_C, with the characteristic frequency shift of the modes described as $\Delta\omega_c \sim (T_C - T)^{0.5}$ [7, 8]. As to the PT at T_s, no anomaly in the frequency shift or damping of the IR-active soft mode [7] or in the damping

0953-8984/98/419309+08$19.50

of the acoustic shearing mode [9] in the vicinity of T_s was revealed. The Raman-active soft mode which could be related to the PT at T_s has not been detected. Although at 165 K the low-frequency Raman-active mode was observed (at about 5 cm^{-1}) [8], no reliable data about the emergence of the mode either below T_s or below T_C or about the temperature dependence of its frequency shift was presented.

The EPR line splitting was reported to occur below T_C both for $Cd_2Nb_2O_7$ doped with Cr^{3+} (electron spin $S = 3/2$, ground state $^4F_{3/2}$) [10] and for $Cd_2Nb_2O_7$ doped with Gd^{3+} (electron spin $S = 7/2$, ground state $^8S_{7/2}$) [11] for $\boldsymbol{B}_0 \| [111]_{cub}$, while the EPR spectra for other orientations of the external magnetic field, $\boldsymbol{B}_0$, were not studied.

To give insight into the spin–lattice interactions, the lattice dynamics and the evolution of the ferroic states below T_s and T_C, we focus on the EPR spectroscopy (using Gd^{3+} as the EPR probe) and optical microscopy study of $Cd_2Nb_2O_7$ pyrochlore since these methods provide information about the behaviour of the system on a temperature scale and a spatial scale.

2. Experiment

Nominally 'pure' single crystal samples of $Cd_2Nb_2O_7$ and those doped with Gd^{3+} (<0.05 at.%) were studied in the temperature interval of 80 K $< T <$ 300 K which included PTs at T_s, T_C and T_{inc} (=86 K), with the phase below T_{inc} specified as an incommensurate one [5]. The single crystals were grown by the flux method [1, 12, 13]. The different colours of the nominally 'pure' crystals of different batches (colourless, yellow, orange or red-orange) are due to random substitution of transition-metal ions (TM) for Cd^{2+} [12, 14, 15]. Nevertheless, for less than 0.1 at.% of the substituted ions, neither the sequence of PT in $Cd_2Nb_2O_7$ pyrochlore nor the PT temperature points change noticeably [5, 6, 12, 14].

As-grown $(111)_{cub}$ colourless platelets were preferred for optical microscopy studies. The platelets of this crystallographic orientation were chosen to draw an analogy with the EPR data. The colourless platelets were chosen to exclude the effect of defects and impurities on pinning or facilitating the domain wall motion [16]. The samples of about 10 mm^2 in area and less than 0.5 mm in thickness were investigated with the experimental set-up described in [3]. In view of the photosensitivity of the crystals [17] and of the easy switching of the domains of both ferroic phases under illumination [18], the optical experiments were carried out in the 'light off' regime. In this regime, the sample was illuminated only during photographing of the domain pattern at a few fixed temperatures on cooling and heating, with the exposures shorter than 2 s. This method enabled us to observe a true thermally driven domain pattern on a spatial scale and to correlate these data with the EPR data obtained without illumination of the sample.

A conventional EPR method was used to obtain information about the nature and the evolution of ferroic states on a temperature scale as well as about thermally induced or dc electric field-induced changes in the relative macroscopic volume occupied by ferroic domains (see also [10, 19, 20]). The EPR spectra were obtained both for parallel and perpendicular orientation of the external magnetic field relative to the $[111]_{cub}$-type direction. This crystallographic direction corresponds to the principal z-axis for the gradient of the crystal field acting on the Gd^{3+} ion (D_{3d}-3m site symmetry).

The spin Hamiltonian used to describe the Gd^{3+} EPR spectra is written in the form [11]

$$H = g\beta BS + b_2^0 O_2^0 + b_4^0 O_4^0 + b_6^0 O_6^0 + b_4^3 O_4^3 + b_6^3 O_6^3 + b_6^6 O_6^6 \qquad (1)$$

where b_n^m are the crystal field parameters, O_n^m are the Steven's operators of the same symmetry. Both b_n^m and O_n^m are angular dependent, $b_n^m = f(\theta, \varphi)$ and $O_n^m = f(\theta, \varphi)$,

where φ is the polar angle and θ is the azimuth angle for the $\boldsymbol{x}$-, $\boldsymbol{y}$-, $\boldsymbol{z}$-axes of the crystal field gradient.

This spin Hamiltonian can be also used to describe the Cr^{3+} EPR spectra, with the parameter b_2^0 being the only non-zero one. In the case of Gd^{3+}, the b_4^0, b_4^3 and b_6^6 parameters in the equation are non-zero, too.

If θ and $\varphi = 0^\circ$ ($\boldsymbol{B}_0 \| [111]$) b_6^6 is equal to zero. As a result, for $\boldsymbol{B}_0 \| [111]$ the Gd^{3+} EPR line splitting is observed at T_C, while for Cr^{3+} the EPR line splitting is observed at T_C both for $\boldsymbol{B}_0 \| [111]$ and $\boldsymbol{B}_0 \perp [111]$ [10]. If $\theta = 90^\circ$ ($\boldsymbol{B}_0 \perp [111]$), $b_6^6 \neq 0$. In this case, an additional Gd^{3+} EPR line splitting ($+5/2 \rightarrow +3/2$) is observed at T_s. This means that using Gd^{3+} as the EPR probe one can study the dependence of the line separation, ΔB, and, therefore, of the order parameter at the structural PT, η, on temperature both below T_s and T_C. Then, the critical order-parameter index, β, that characterizes the structural PT can be estimated using the $\Delta B \sim \eta_1 \sim (T_s - T)^\beta$ or $\Delta B \sim \eta_2 \sim (T_C - T)^\beta$ formula, respectively [21]. The intensity ratio of the split lines characterizes thermally induced or dc electric-field-induced changes in the domain pattern below T_s and T_C [10, 19, 20].

3. Results

3.1. The EPR study of PT in $Cd_2Nb_2O_7$ doped with Gd^{3+}

On partial substitution of Gd^{3+} for Cd^{2+}, an excess charge is compensated by the O^{2-} (7th) ion due to the unusual position of this ion in the pyrochlore structure [12] and due to high polarizability of the oxygen ions. To analyse the EPR spectra, the characteristic fine-structure spin-Hamiltonian parameters for the Gd^{3+} ion estimated in [11] are used.

Figure 1 presents the temperature dependence of the EPR line splitting and of the magnetic resonance field for the split lines. When $\boldsymbol{B}_0 \perp [111]$, the ($\pm 5/2 \leftrightarrow \pm 3/2$) EPR line splitting provides information about the temperature-dependent order parameters η_1 and η_2.

When $\boldsymbol{B}_0 \| [111]$, the single EPR line ($5/2 \leftrightarrow 3/2$) in the spectrum in the paraelectric–paraelastic phase ($T_s < T < 300$ K) splits into two components just below T_C, as for Cr^{3+} [10]. The line splitting is well fitted with the $\Delta B \sim (T_C - T)^\beta$ formula, with the critical index $\beta = 0.5$, which is typical of a proper PT [21]. When $\boldsymbol{B}_0 \perp [111]$, the line splitting occurs both below T_s (the lines A and D) and below T_C (the lines B and C). This proves the crystal-field symmetry breaking to take place not only at T_C, but also at T_s. Below T_s, the line splitting changes as $\Delta B \sim (T_s - T)^\beta$ with $\beta = 1$, which is characteristic of an improper PT [21]. Below T_C, the line splitting changes as $\Delta B \sim (T_C - T)^\beta$ with $\beta = 0.5$, which conforms to the behaviour of the Raman-active soft mode [8] and is typical of a proper PT [21]. Finally, from the structure-instability viewpoint (taking into account also the nature of the ferroic states [3–5]), the state of the system below T_s can be characterized as an improper ferroelastic, while the state of the system below T_C can be characterized as a proper ferroelectric–ferroelastic.

In the case of $\boldsymbol{E}_{dc} \| \boldsymbol{B}_0 \perp [111]$, the change in the intensity ratio of the split lines A and D, A/D, enables us to trace the evolution of the ferroelastic domains on coming to the ferroelectric phase (figure 2). At $E_{dc} = 0$, the strong unipolarity of the system in the ferroelectric phase (A $\neq$ D) is due to the strong intrinsic bias field. At $E_{dc} \neq 0$, the intensity ratio of the lines A and D reverses on a temperature scale with reversing the direction of the $\boldsymbol{E}_{dc}$-field. This implies that below T_C the domains of the improper ferroelastic phase manifest ferroelectric features, too. Thus, two ferroic states of different nature (an improper ferroelectric–ferroelastic state and a proper ferroelectric–ferroelastic state, with the latter

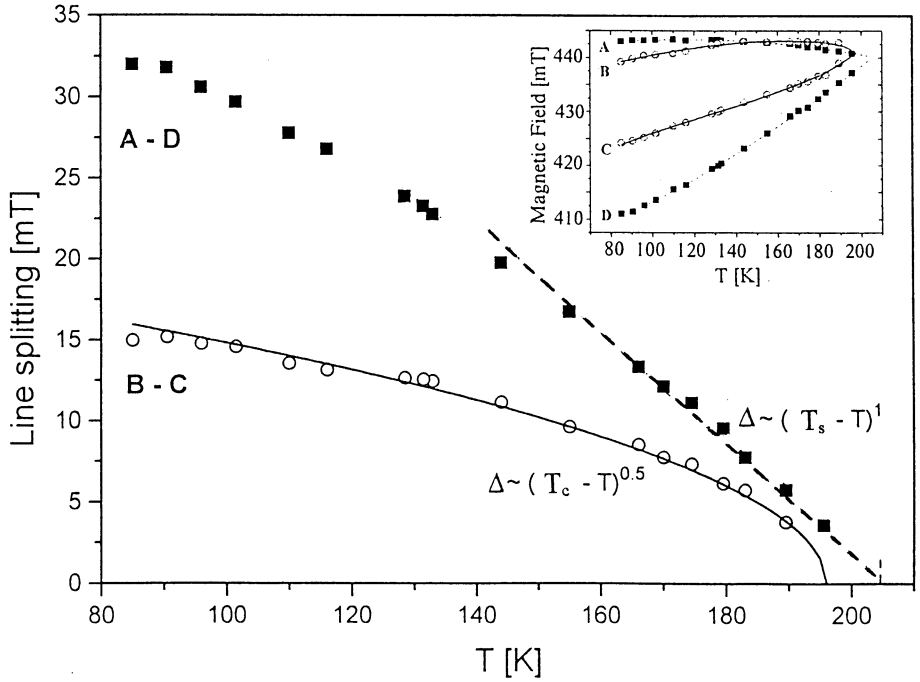

Figure 1. The EPR line splitting for $Cd_2Nb_2O_7 : Gd^{3+}$ below T_s and T_C for $\boldsymbol{B}_0 \perp [111]_{cub}$. The inset shows the magnetic resonance field versus temperature dependence for the split lines.

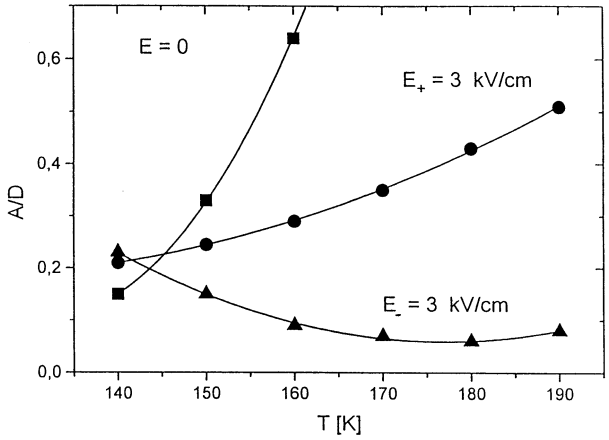

Figure 2. The temperature dependence of the intensity ratio of the EPR split lines A and D for a few dc electric field strengths in the ferroelectric phase ($\boldsymbol{E}_{dc} \| \boldsymbol{B}_0 \perp [111]_{cub}$).

appearing below T_C) coexist in the ferroelectric phase, at least down to the next PT at T_{inc}. In other words, to describe the state of the system below T_C, a multiple-component primary order-parameter should be chosen. The coexistence of two ferroic states of different nature in the ferroelectric phase of $Cd_2Nb_2O_7$ is also confirmed by the optical microscopy study (section 3.2).

3.2. The evolution of domains on a temperature scale and a spatial scale

Here, the domain pattern in the ferroelectric phase of $Cd_2Nb_2O_7$ is studied in the 'light off' regime, which has never been done before for photosensitive materials. The aim of the study is (i) to clarify the physical origin for coexistence of the $[100]_{cub}$-type domains and the $[110]_{cub}$-type domains below T_C, and (ii) to obtain information about true thermally induced changes in the domain pattern since they influence dielectric permittivity, specific heat, the EPR split line intensity etc. Besides, the contradiction in the behaviour of domains in the illuminated samples with decreasing temperature reported in previous works [1–4, 18] needs to be eliminated. On the study of the domain pattern in $Cd_2Nb_2O_7$ with a conventional optical microscopy method (i.e., in the 'light on' regime), the $[110]_{cub}$-type domains were usually observed to decrease in number with decreasing temperature [1, 3, 4, 18], while according to [2] the domains increased in number with decreasing temperature.

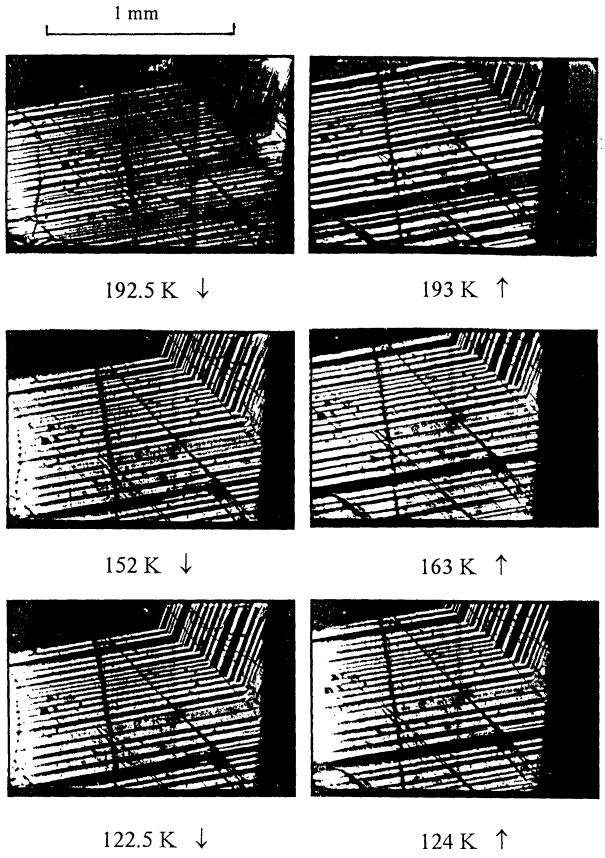

Figure 3. The thermally-induced evolution of domains of two ferroic phases in the $(111)_{cub}$ colourless platelet in the 'light off' regime (magnified by 41×). Cooling (left) and heating (right) rate was 15 K min^{-1}. Before heating the sample was cooled down to 78 K.

The domain pattern developed in the $(111)_{cub}$ platelet below T_C is most complicated (figure 3). Indeed, the projections of the domain walls along the $[100]_{cub}$ and $[110]_{cub}$-type directions are lying along the same $[112]_{cub}$-type directions, which makes the projections inseparable [1–4, 12]. Moreover, each $[110]_{cub}$ and $[112]_{cub}$-type direction in this plane twins.

The domain pattern of the improper ferroelastic phase ($T_C < T < T_s$) consists of uniformly coloured dark and light stripes. The border between these stripes is diffused and irregular. Below T_C, the stripes disintegrate to the wedge-shaped domains of different colours arranged for a succession of colour orders. Within 160 K $< T < T_C$, some wedge-shaped domains narrow and gradually disappear, while others are detected optically down to T_{inc}. On heating in the 'light off' regime, the former does not reappear up to T_s, while the latter is restored on approaching T_C. The same scenario is played every time when the thermal scan is repeated starting from $(T_s + \Delta T)$, where $\Delta T \geqslant 20$ K, with the sample kept at this temperature for about one hour.

Although at $T < 160$ K some domains become indistinguishable with the optical microscopy method (figure 3), over the whole temperature region of $T_{inc} < T < T_C$ the domains are easily switched by dc electric field or uniaxial stress [1, 3, 4] (see also section 3.1 and figure 2). These facts imply that over the temperature region of $T_{inc} < T < T_C$ (i) the domains are simultaneously ferroelectric and ferroelastic, yet (ii) the nature of domains is different. In view of these findings and the results presented in section 3.1, one may conclude that the state of the system appearing below T_C is a proper ferroelectric–ferroelastic, whereas an improper ferroelastic state appearing below T_s is converted into an improper ferroelectric–ferroelastic state below T_C.

Below T_s, the state of the system is characterized by Aizu species $\{m3mFmmm(\mathrm{pp})\}$ as a full ferroelastic [22]. Below T_C, the state of the system is characterized by Aizu species $\{m3mFmm2(\mathrm{pp})\}$ as a partial ferroelectric–partial ferroelastic [4, 22].

4. Discussion

On the basis of the Gd^{3+} EPR spectroscopy and optical microscopy studies, the following scheme for the evolution of the states in $Cd_2Nb_2O_7$ pyrochlore on a temperature scale can be suggested. The primary improper ferroelastic state appearing below T_s is converted into an improper ferroelectric–ferroelastic state below T_C. Irrespective of this state, a proper ferroelectric–ferroelastic state appears below T_C. Both states coexist in the ferroelectric phase down to the next PT at T_{inc}, with domains of the improper ferroelectric–ferroelastic state being observed optically only within 160 K $< T < T_C$. The coexistence of two ferroic states of different nature in the ferroelectric phase implies that at least a two-component primary order parameter should be used to describe the state of the system below T_C.

The fact that the PT to an improper ferroic state starts a sequence of PTs in $Cd_2Nb_2O_7$ pyrochlore (see also [5]) deserves special attention. According to [21], this means that below T_s distortions in the low-symmetry phase do not break as many of the symmetry elements of the high-symmetry phase ($Fd3m$–O_h^7) as would be broken by a proper ordering of the system described by the primary order parameter. Indeed, below T_s the cubic point group of the high-symmetry phase, $m3m$, is distorted to the orthorhombic point group, $mmm(\mathrm{ss})$, while below T_C the orthorhombic point group $mmm(\mathrm{ss})$ changes only to the orthorhombic point group $mm2(\mathrm{pp})$ (section 3.2 and [4]). Nevertheless, although immediate symmetry breaking from $m3m$ to $mm2(\mathrm{pp})$ in $Cd_2Nb_2O_7$ is hindered, a tendency to this symmetry distortion is inherent in the structure [3–5].

To understand the mechanism for stepped symmetry breaking and for the coexistence of ferroic states in $Cd_2Nb_2O_7$, one has to take into account that the pyrochlore structure can be described as two interpenetrating networks [6, 10, 23, 24]. The rigid structural framework is composed of the $(NbO_6)^{n-}$ coordination polyhedra sharing their corners around hexagonal vacancies (figure 4). The vacancies are occupied by the O (7th)–Cd–O (7th) dipole chains constituting the second network. The bonding between the Cd ion and six equally spaced

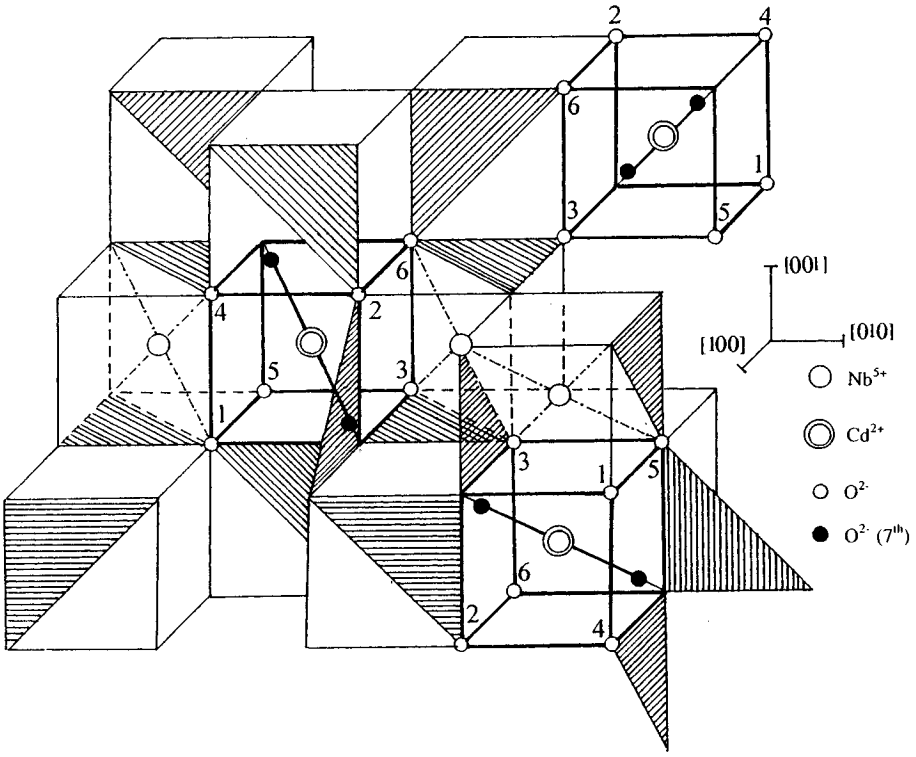

Figure 4. The schematic image of the pyrochlore structure in the case of $Cd_2Nb_2O_7$ pyrochlore composed of two weakly-bonded networks. One of the networks is formed by the $(NbO_6)^{n-}$ trigonal antiprisms, the other is formed by the O (7th)–Cd–O (7th) dipole chains.

oxygen ions which belong simultaneously to the $(NbO_6)^{n-}$ and $(CdO_8)^{n-}$ coordination polyhedra is rather weak in comparison with that between the Cd ion and the two oxygen ions in the chains because of a significant difference in the bond lengths (0.263 nm and 0.225 nm, respectively) [12, 23–25]. For this reason, the former is ignored sometimes when the pyrochlore structure is described [23]. Besides, the ionic size of Cd^{2+} is the smallest one permitted for a cation in the A position [12], so that the stability of the pyrochlore structure is ensured by the dynamic location of Cd^{2+} ions in the central position of the $(CdO_8)^{n-}$ polyhedra [25]. At PT, a distortion in the shape of the $(NbO_6)^{n-}$ polyhedra induces a distortion in the O (7th)–Cd–O (7th) dipole chains, too. However, in the case of $Cd_2Nb_2O_7$ pyrochlore the second network is involved in the distortion process with delay because of a relatively weak bonding between two networks. As a result, instead of a single PT, two PTs (at T_s and T_C) close together on a temperature scale are displayed in the system. The weak bonding between the networks is expected to be responsible for different physical states in the different networks. Taking into account the different behaviour of two weakly-bonded networks, one can explain the coexistence and evolution of the ferroic states of different nature in the ferroelectric phase of $Cd_2Nb_2O_7$ (section 3). Besides, one can also explain the coexistence of the ordered (ferroelectric) and disordered (relaxor, incommensurable, glassy) states in this compound reported in [5] and [6]. To obtain more information about the role of two weakly-bonded networks in the appearance and evolution of the physical states in

$Cd_2Nb_2O_7$, other studies of mixed compounds in which the rare-earth or transition-metal ions are partially substituted for Cd^{2+} need to be performed.

5. Conclusions

Gd^{3+} EPR spectroscopy and optical microscopy studies of $Cd_2Nb_2O_7$ pyrochlore were carried out within the temperature range of 80 K–300 K which includes the PTs at T_s, T_C and T_{inc}. The evidence for coexistence of the ferroic states of different nature in the ferroelectric phase of $Cd_2Nb_2O_7$ is presented. Unlike previous observations [1–4], the domains of an improper ferroelectric–ferroelastic state in the 'light off' regime are observed optically over a wider temperature interval, i.e. down to 160 K. The unusual behaviour of the system on a temperature scale and a spatial scale is ascribed to the different roles of two weakly-bonded networks in the appearance and evolution of the physical states in $Cd_2Nb_2O_7$. This mechanism seems to be also responsible for the coexistence and evolution of the ordered (ferroelectric) and disordered (relaxor, incommensurable, glassy) states in this compound reported in [5] and [6].

Acknowledgment

Financial support from the Russian Foundation for Basic Researches under grant RFFI-9702-18099 is gratefully acknowledged.

References

[1] Golovshchikova G I, Isupov V A and Myl'nikova I E 1971 *Fiz. Tverd. Tela* **13** 2349
[2] Salaev F M, Kamzina L S, Krainik N N, Sher E S and Smolensky G A 1983 *Fiz. Tverd. Tela* **25** 163
[3] Kolpakova N N, Margraf R and Pietraszko A 1987 *Fiz. Tverd. Tela* **29** 2638
[4] Ye Z G, Kolpakova N N, Rivera J-P and Schmid H 1991 *Ferroelectrics* **124** 275
[5] Kolpakova N N, Wiesner M, Shul'pina I L, Szczepan'ska L and Piskunowicz P 1996 *Ferroelectrics* **185** 131
[6] Kolpakova N N, Wiesner M, Kugel G and Bourson P 1997 *Ferroelectrics* **190** 179
Kolpakova N N, Wiesner M, Kugel G and Bourson P 1997 *Ferroelectrics* **201** 107
[7] Banys J, Grigas J, Kolpakova N N, Sobestijanskas R and Sher E 1989 *Lithuanian J. Phys.* **29** 209
[8] Smolensky G A, Kolpakova N N, Kizhaev S A and Siny I G 1982 *Ferroelectr. Lett.* **44** 129
[9] Yushin N K and Smirnov S I 1986 *Fiz. Tverd. Tela* **28** 3161
[10] Waplak S and Kolpakova N N 1990 *Phys. Status Solidi* a **117** 461
[11] Geifman J N, Sirotkin G W and Sher E S 1983 *Fiz. Tverd. Tela* **25** 3606
[12] Jona F, Shirane G and Pepinsky R 1955 *Phys. Rev.* **98** 903
[13] Aleshin E and Roy R 1962 *J. Am. Ceram. Soc.* **45** 18
[14] Minge J, Waplak S and Kolpakova N N 1991 *Mater. Sci.* **17** 41
[15] Kolpakova N N, Wiesner M, Lebedev A O, Syrnikov P P and Khramtsov V A 1998 *Tech. Phys. Lett.* at press
[16] Bornarel J 1972 *J. Appl. Phys.* **43** 845
Bornarel J 1995 *Ferroelectrics* **172** 53
[17] Kolpakova N N, Ye Z G, Rivera J-P, Schmid H and Verentchikova R G 1993 *Ferroelectrics* **143** 171
[18] Kolpakova N N, Polomska M and Hilczer B 1994 *Abstract Book ISFD-3 (Zakopane 1994)* (Poznan: Polish Academy of Sciences) p 2:08
[19] Waplak S and Stankowski J 1978 *Acta Phys. Polon.* A **54** 465
[20] Jerzak S, Waplak S and Shuvalov L A 1982 *Phys. Status Solidi* a **72** 783
[21] Bruce A D and Cowley R A 1981 *Structural Phase Transitions* (London: Taylor and Francis)
[22] Aizu K 1970 *Phys. Rev.* B **2** 754
Aizu K 1969 *J. Phys. Soc. Japan* **27** 387
[23] Sleight A W 1969 *Inorg. Chem.* **8** 2039
Sleight A W 1968 *Inorg. Chem.* **7** 1704
[24] McCauley R A 1980 *J. Appl. Phys.* **51** 290
[25] Lukaszewicz K, Pietraszko A, Stepien-Damm J and Kolpakova N N 1994 *Mater. Res. Bull.* **29** 987